# A New Graphic Plot Analysis for Cerebral Blood Flow and Partition Coefficient with Iodine-123-Iodoamphetamine and Dynamic SPECT Validation Studies Using Oxygen-15-Water and PET

Takashi Yokoi, Hidehiro Iida, Hiroshi Itoh and Iwao Kanno

*Department of Research for Nuclear Medicine, Medical Systems Division, Shimadzu Corporation, Kyoto, Japan and Department of Radiology and Nuclear Medicine, Research Institute for Brain and Blood Vessels, Akita, Japan*

To estimate regional cerebral blood flow (rCBF) and brain-blood partition coefficient ($\lambda$) using a dynamic measurement, a new graphic plot analysis is proposed. By assuming a two-compartment model for tracer kinetics, we derived the linear relationship as $Y(t) = K_1 - k_2 X(t)$, where Y(t) is the ratio of brain tissue activity-to-time-integrated arterial blood activity and X(t) is the ratio of time-integrated brain tissue activity-to-time-integrated arterial blood activity. A plot of Y(t) against X(t) yields a straight line and the y- and x-intercept of the regression line represent rCBF ($K_1$) and $\lambda$, respectively. The slope is a washout constant ($-k_2$). This method was applied to 14 subjects with N-isopropyl-p-iodine-123 iodoamphetamine ([$^{123}$I]IMP). The mean values of $K_1$ and $\lambda$ for normal subjects were 41.3 ± 6.7 ml/100 g/min and 29.6 ± 6.5 ml/g, respectively, in the gray matter. A comparative study with positron emission tomography (PET) using an $H_2{}^{15}O$ autoradiographic method revealed good correlation between IMP $K_1$ and PET rCBF [r = 0.822; $K_1$ = 0.842 rCBF + 0.030 (ml/g/min)]. The values of $K_1$ using the graphical method were in excellent agreement with those using a nonlinear least-squares fitting technique (r = 0.992 for $K_1$; r = 0.941 for $\lambda$). The estimated $K_1$ values in the graphical method were not changed when scanning times were varied. We conclude that a two-compartment model is acceptable for IMP kinetics within a scan time of 60 min. The graphical method gives a reliable and rapid estimation of rCBF when applied to dynamic data.

**J Nucl Med 1993; 34:498–505**

Received Apr. 30, 1992; revision accepted Oct. 7, 1992.

For correspondence or reprints contact: Takashi Yokoi, Dept. of Research for Nuclear Medicine, Medical Systems Division, Shimadzu Corporation, 1 Nishinokyo-Kuwabaracho Nakagyo-ku, Kyoto 604, Japan

N-isopropyl-p-iodine-123-iodoamphetamine ([$^{123}$I]IMP) (*1*) can be used to quantify rCBF using single-photon emission computed tomography (SPECT) (*2–5*). Kuhl et al. (*2*) estimated rCBF with a microsphere model neglecting the washout from the brain. However, the microsphere model underestimated rCBF with increasing scan duration because of the influence of washout (*6*). Greenberg et al. (*5*) showed that [$^{123}$I]IMP was a rCBF indicator from comparative studies using PET and $H_2{}^{15}O$. They used a two-compartment model for [$^{123}$I]IMP with a nonlinear least-squares fitting technique.

We developed a new graphic plot method based on a two-compartment model for rapid, simultaneous estimation of rCBF and partition coefficients. The purpose of this study is to validate the graphical method. This method was applied to dynamic data from human studies with [$^{123}$I]IMP. A comparative study with PET and $H_2{}^{15}O$ was performed to validate the new graphical method. The accuracy of the present method was compared with the conventional nonlinear least-squares fitting technique.

## THEORY

Iodine-123-IMP was assumed to be freely diffusible from blood pool to brain tissue, and thus it was possible to be described by a two-compartment model. This can be written by a first-order differential equation (*7*):

$$\frac{dC_b(t)}{dt} = K_1 C_a(t) - k_2 C_b(t), \qquad \text{Eq. 1}$$

where $C_a(t)$ and $C_b(t)$ are the decay-corrected radioactivity concentration in arterial blood ($\mu$Ci/ml) and brain tissue ($\mu$Ci/g), respectively. $K_1$ is the rCBF (ml/g/min) and $k_2$ is the washout constant ($min^{-1}$) from the brain. Brain tissue-blood partition coefficient is defined as $\lambda = K_1/k_2$ (ml/g).

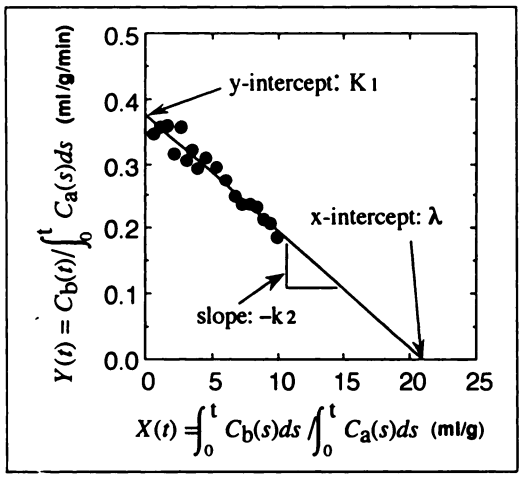


**FIGURE 1.** An illustration of the present graphic method. The y- and x-intercept of the regression line represent $K_1$ (ml/g/min) and $\lambda$ (ml/g), respectively. The slope of the line represents the $-k_2$ ($min^{-1}$).

The integration of Equation 1 gives the following equation:

$$C_b(t) = K_1 \int_0^t C_a(s)ds - k_2 \int_0^t C_b(s)ds. \quad \text{Eq. 2}$$

The terms of $\int_0^t C_a(s)ds$ and $\int_0^t C_b(s)ds$ are integral data from 0 until a certain time t. By dividing both sides of Equation 2 by $\int_0^t C_a(s)ds$, the following linear relationship is derived:

$$Y(t) = K_1 - k_2X(t) \quad \text{Eq. 3}$$

where

$$X(t) = \frac{\int_0^t C_b(s)ds}{\int_0^t C_a(s)ds}, \text{ and } Y(t) = \frac{C_b(t)}{\int_0^t C_a(s)ds}.$$

The plot of Y(t) against X(t) yields a straight line with a slope of $-k_2$ ($min^{-1}$) and a y-intercept equal to $K_1$ (ml/g/min). Therefore, the x-intercept of the line represents the partition coefficient $\lambda$ (ml/g). Figure 1 illustrates the basic idea of the graphical method. This method enables rapid estimation of both $K_1$ and $\lambda$ using standard linear regression analysis.

## METHODS

### Subjects

IMP-SPECT studies were performed on 14 subjects: five normal subjects and nine patients with cerebrovascular disease (CVD). Five of these underwent PET measurements with $H_2{}^{15}O$ on the same day except for one patient, where there was a 5-day interval.

### SPECT Measurements and Data Analysis

A dose of 6 mCi [$^{123}$I]IMP (Nihon Medi+Physics, Takarazuka, Japan) ($^{123}$I produced by the [p, 5n] reaction, $^{124}$I free) was administered into a cubital vein over 1 min. Dynamic scans were performed (9 scans of 2 min, 9 scans of 4 min and 1 scan of 3 min; total 57 min) after the intravenous injection and then a delayed scan was collected at 210 min. Images were acquired using the HEADTOME-II (*8,9*) (Shimadzu Corporation, Kyoto, Japan) with three simultaneous slices at 35-mm intervals. Images were reconstructed on a 64 × 64 matrix using filtered backprojection with a Butterworth filter. An effective spatial resolution at the center of field of view was 12 mm FWHM, and the slice thickness was 17 mm. Attenuation correction was made numerically by assuming an elliptical brain outline. The head of the patient was parallel to the orbitomeatal line (OM line), and the lower slice of SPECT scanner was adjusted to 7 mm above the OM line. A headholder was used to minimize subject movements.

Arterial blood was sampled from the radial artery with the following protocol: every 15 sec for the first 90 sec, every 30 sec for the next 6 min, and then gradually increasing the sampling interval for a total of 25 samples. Arterial blood activity was measured with a well-counter calibrated to the SPECT scanner. To obtain a cross-calibration factor, a cylindrical phantom (16 cm diameter and 15 cm length) filled with $^{123}$I solution (1 mCi) was scanned for 10 min and then a known volume of activity from the phantom was measured using the well-counter. This provided the cross-calibration factor between cps/pixel from the tomographic images and cps/ml obtained from the well-counter. The concentration of unmetabolized IMP was determined using an octanol extraction.

Brain tissue activity curves (counts/pixel) were obtained from regions of interest (ROIs) on dynamic images. Actual brain tissue concentrations were not measured as instantaneous values $C_b(t)$, but as integrals over the duration of a single scan. To obtain the $C_b(t)$ (cps/pixel), the measured integral data were normalized for the scan duration (sec). We used the normalized $C_b(t)$ as instantaneous values at midtime t. These values were converted to an equivalent well-counter (cps/ml) using the calibration factor. The arterial blood data $C_a(t)$ and brain tissue data $C_b(t)$ were corrected for the physical decay of $^{123}$I (13 hr) and were then integrated to calculate the $\int_0^t C_a(s)ds$ and $\int_0^t C_b(s)ds$. The integral blood data were interpolated at the respective midtime of each serial scan. The values of $K_1$ and $\lambda$ were calculated according to Equation 3 using linear regression analysis. To avoid the influence of cerebral blood volume, we did not use the first data in the linear fitting. The analysis was accomplished on a Macintosh® SE/30 (Apple Computer, Inc., Cupertino, CA) using Excel® software (Microsoft Corp.).

To evaluate the accuracy of the graphical method, the values of $K_1$ and $\lambda$ were compared to those by a nonlinear least-squares fitting technique with a simple algorithm. We also estimated $K_1$ using the microsphere model based on the operational equation:

$$K_{1\ \text{microsphere}} = \frac{C_b(T)}{\int_0^T C_a(t)dt}, \quad \text{Eq. 4}$$

where T is the scan time. The estimated $K_{1\ \text{microsphere}}$ is identical to Y(T) in the graphical method (Equation 3).

### PET Measurements and Data Analysis

Measurements of CBF using PET and $H_2{}^{15}O$ were performed before the SPECT studies. After the transmission scan was carried out for 6 min to correct tissue attenuation, an intravenous bolus injection of $H_2{}^{15}O$ (0.6 mCi/body weight in kg) was given and a 90-sec scan was obtained. Images were acquired using the HEADTOME-IV (*10,11*) (Shimadzu Corporation, Kyoto, Japan) with 14 tomographic images at intervals of 6.5 mm from the continuous axial motion (Z-motion) of the gantry. Image reconstruction was performed on a 128 × 128 matrix using the filtered backprojection technique with a ramp function and Butterworth filter. An effective spatial resolution was 9.0 mm FWHM, and the slice thickness was 10 mm FWHM. Total counts in the image were 600–800 × $10^3$ per slice. The deadtime and radioactivity decay were corrected on-line (*12,13*). The patient's head was parallel to the OM line, and the lower slice of PET scanner was adjusted to 7 mm above the OM line.

Arterial blood radioactivity was monitored from a radial artery using a $\beta^+$ detector with a plastic scintillator (*14*). Arterial blood was withdrawn at a rate of 5 ml/min and was sampled at 1-sec intervals. The internal dispersion of the measured arterial blood data was corrected within 3 sec (*15*). The cross-calibration between the $\beta^+$ detector and the PET scanner was carried out using a well-counter after each study. Details of the blood sampling system have been previously described (*15,16*). The rCBF images were calculated using the operational equation of the table lookup method (*17–19*) with a $\lambda$ of 0.90 ml/g for water.

### Definition of ROIs

ROI analyses were done by an experienced radiologist on a graphic workstation (TITAN-750, Stardent Computer Inc., MA) using the software package DR. VIEW (Asahi Chemical Inc., Tokyo, Japan). The pixel size of SPECT images (3.28 × 3.28 mm/pixel in 64 × 64 matrix) was adjusted to that of PET-rCBF images (2.0 × 2.0 mm/pixel in 128 × 128 matrix), and then the PET-rCBF images were manually moved to adjust the position of SPECT images. Elliptical ROIs (16 mm in short-axis, 32–64 mm in longaxis) were defined on the PET-rCBF images as a reference in the cerebellum, temporal cortex, frontal cortex and parietal cortex in each of the two hemispheres. Selected slices were OM +7.0 mm (cerebellum), +42.0 mm (temporal and frontal cortex) and +77.0 mm (parietal cortex) in SPECT. Corresponding slices were OM +7.0, +39.5 and +78.5 mm in PET. Time-activity curves of IMP-SPECT data were generated from the ROIs and were transferred to the Macintosh to estimate the values of $K_1$ and $\lambda$ using the graphical method.

### Computer Simulations

We evaluated the effect of tissue heterogeneity (*20*) caused by limited spatial resolution using a computer simulation. Heterogeneous tissue curves were generated as a mixture of the two components for gray matter ($K_1$ = 80 ml/100 g/min, $\lambda$ = 30 ml/g) and white matter ($K_1$ = 20 ml/100 g/min, $\lambda$ = 30 ml/g). The simulation was performed for two cases: where the fraction of gray matter was varied from 0 to 100% with the scan duration of 60 min and where the scan duration was varied from 0 to 210 min with the 50% gray matter fraction.

In the simulations, the arterial input curve used was derived from typical data acquired from a human study and the brain tissue curves were generated by the numerical solution of the differential equation using a fourth-order Runge-Kutta procedure with a time step of 15 sec.

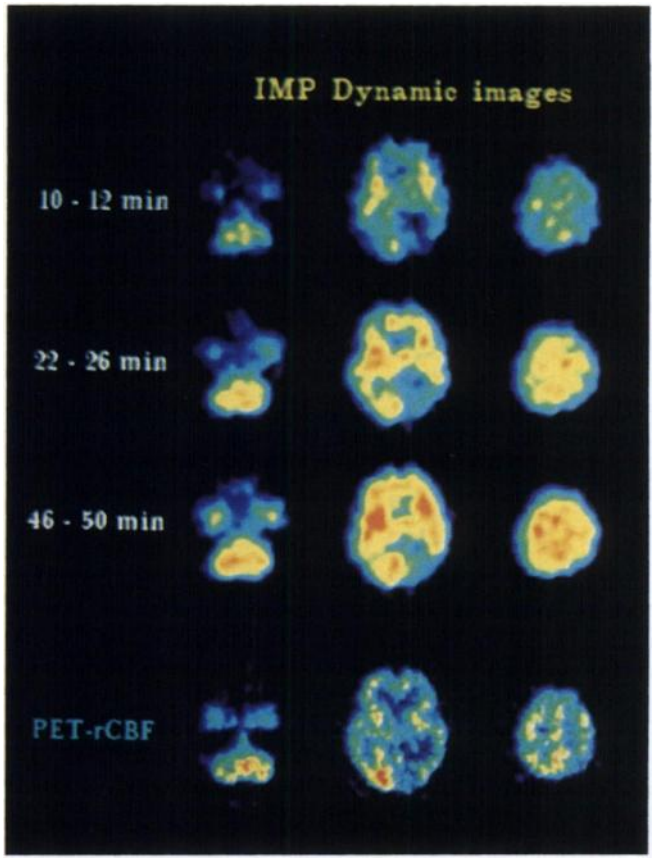


**FIGURE 2.** Corresponding IMP-SPECT and PET images in a patient with CVD (P7 in Table 1). The dynamic IMP images were measured from 10–12 min, 22–26 min and 46–50 min after intravenous injection of IMP. The PET-rCBF images were calculated using an $H_2{}^{15}O$ autoradiographic method. Selected slices were OM+7.0, +42.0, and +77.0 mm in SPECT, and OM+7.0, +39.5 and +78.5 mm in PET.

## RESULTS

### Graphic Plot Analyses

Figure 2 shows the corresponding IMP-SPECT and $H_2{}^{15}O$-PET images in a patient with CVD. Figure 3 shows the time course of the measured arterial blood and brain tissue activity in the same subject. Figure 4 illustrates the scatter plots of Y(t) against X(t) according to Equation 3. The y- and x-intercept of the regression line provide the rCBF $K_1$ (ml/g/min) and $\lambda$ (ml/g), respectively, and the slope represents the $-k_2$ ($min^{-1}$). The delayed scan data were slightly larger than the predicted values from the regression line.

Table 1 shows the values of $K_1$ in normal subjects (N1–N5) and patients (P1–P9) using IMP-SPECT. The mean values of $K_1$ were 41.3 ± 6.7 and 32.4 ± 9.7 ml/100 g/min in the normal subjects (n = 5) and patients (n = 9), respectively. As for $\lambda$, the mean values were 29.6 ± 6.5 and 30.5 ± 10.5 ml/g and the values for the correlation

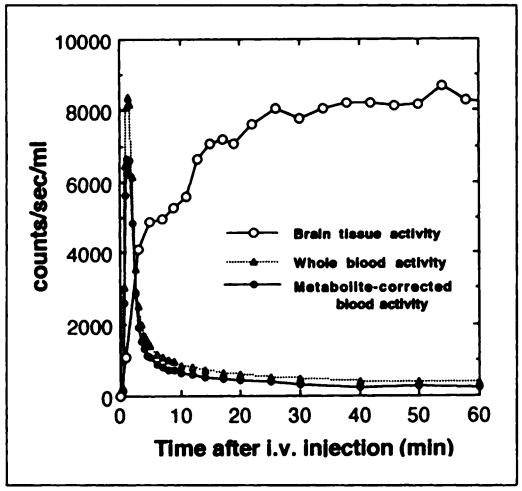


**FIGURE 3.** Time course of activity in whole arterial blood (○) and metabolite-corrected blood (△) following an intravenous injection of [$^{123}$I]IMP in the same subject in Figure 2. Brain tissue activity curve on the right temporal cortex (●) is also shown. All measurements were corrected for physical decay of $^{123}$I.

coefficient between X(t) and Y(t) were −0.924 ± 0.062 and −0.882 ± 0.108 in the normal subjects and patients, respectively. The estimated rCBF values by $H_2{}^{15}O$ autoradiographic method are also shown in Table 1 (N5, P6–P9).

### Correlation Between SPECT and PET

Figure 5 shows a comparison of the values of $K_1$ using IMP-SPECT with the graphical method and the values of rCBF by $H_2{}^{15}O$ autoradiographic method. The correlation between $K_1$ and rCBF was $K_1$ = 0.842 rCBF − 0.030 (ml/g/min), (r = 0.822). A significant correlation was observed, but the mean $K_1$ was slightly lower than the mean rCBF.

### Comparison Estimates Using the Graphical Method and Nonlinear Fitting Technique

Figure 6 shows that the values of $K_1$ and λ obtained using the graphical method were in excellent agreement with those using nonlinear least-squares fitting technique. The correlation in $K_1$ and λ between the two methods in overall regions (112 ROIs) were $K_{1\text{graphical method}}$ = 0.996 $K_{1\text{ fitting}}$ − 0.0003 (ml/g/min), (r = 0.992); $\lambda_{\text{graphical method}}$ = 0.978 $\lambda_{\text{fitting}}$ − 0.103 (ml/g), (r = 0.941). The graphical method was computationally faster than the nonlinear least-squares fitting technique. The graphical method required only a few seconds for application of time-activity data on the Macintosh using Excel, whereas the fitting technique required 20–30 sec on the Macintosh using the C language program.

### Time Dependency of $K_1$ with the Graphical Method and the Microsphere Method

Figure 7 shows the time dependency of $K_1$ with IMP-SPECT using the graphical method and microsphere method in all subjects. The estimated values of $K_1$ using

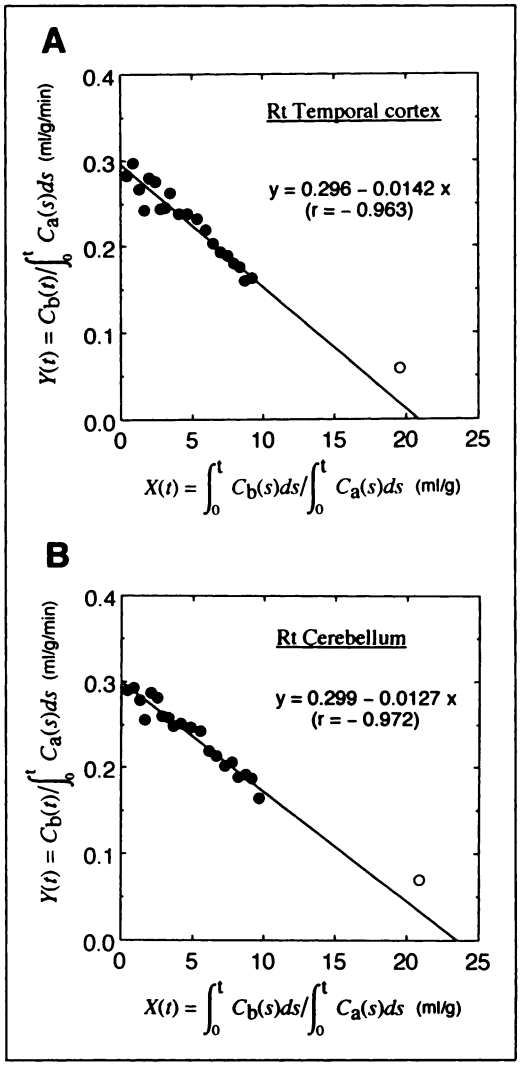


**FIGURE 4.** Typical plots using graphic analysis in (A) the right temporal cortex and (B) the cerebellum from the same subject in Figure 2. The y- and x-intercept of the regression line represent cerebral blood flow $K_1$ and partition coefficient λ (= $K_1/k_2$), respectively. The slope of the line represents $-k_2$. The linear regression analyses were performed using dynamic data obtained from 2 to 57 min (●). The delayed scan data measured at 210 min (○) were also plotted.

the graphical method were almost constant in all ROIs, whereas those using the microsphere model were decreased with an increase in scanning time. The estimated values of $K_1$ using the microsphere model were about 13% lower than those using the graphical method at a scan time of 10 min.

### Computer Simulation Results

Figure 8 shows the errors in $K_1$, $k_2$ and λ due to tissue heterogeneity with a varying gray matter fraction at 60 min. Tissue heterogeneity did not affect the $K_1$, whereas a large underestimation in λ was observed. The maximum error in λ was −27.6% at a 20% gray matter fraction. Figure 9 shows the influence of tissue heterogeneity in

**TABLE 1**
Regional Cerebral Blood Flow Using the Graphical Method with IMP-SPECT and the $H_2{}^{15}O$ Autoradiographic Method

| Patient no. | IMP $K_1$ (ml/100 g/min) | $H_2{}^{15}O$ rCBF (ml/100 g/min) |
|---|---|---|
| N1* | 39.1 | — |
| N2 | 34.4 | — |
| N3 | 46.4 | — |
| N4 | 43.3 | — |
| N5 | 43.4 | 49.1 |
| mean ± s.d. | 41.3 (±6.7) | |
| P1† | 31.2 | — |
| P2 | 38.7 | — |
| P3 | 34.5 | — |
| P4 | 33.2 | — |
| P5 | 37.6 | — |
| P6 | 38.3 | 38.5 |
| P7 | 28.7 | 36.4 |
| P8 | 25.3 | 32.7 |
| P9 | 24.0 | 19.5 |
| mean ± s.d. | 32.4 (±9.7) | |

*N1-5: normal subjects.
†P1-9: patients with cerebrovascular disease. ROIs were defined on the cerebellum, temporal, frontal and parietal cortex in each of the two hemispheres.

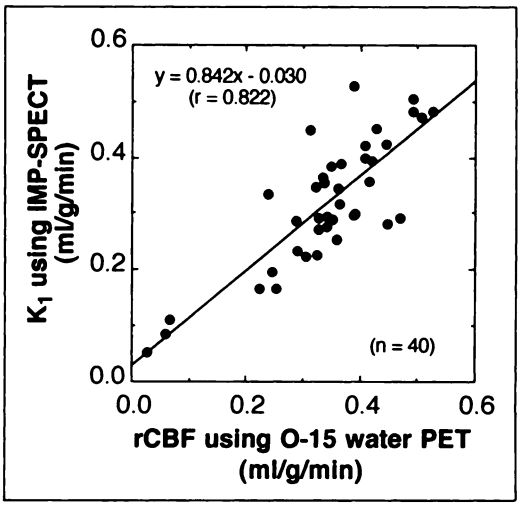


**FIGURE 5.** Correlation of the $K_1$ using IMP and the graphical method with rCBF using $H_2{}^{15}O$ autoradiographic method in five subjects (N5 and P6–P9 in Table 1).

scan times ranging from 0 to 210 min with a 50% gray matter fraction. The regression line was calculated using the data obtained from 0 to 60 min. Linearity between X(t) and Y(t) was maintained up to 60–70 min; however, it became worse with increasing scan time.

## DISCUSSION

We have proposed a new strategy based on graphic plot analysis to estimate $K_1$ and $\lambda$ simultaneously. The graphical method was widely used to estimate cerebral metabolic rate of glucose (CMRglu) using dynamic PET and [$^{18}$F]fluorodeoxyglucose (FDG), the Gjedde-Patlak plot (*21,22*). In the Gjedde-Patlak plot method, the slope of the plotted line is proportional to the CMRglu applied to the three-compartment model ($K_1$-$k_3$). Logan et al. (*23*) estimated the binding potential of the drug with [$^{11}$C]cocaine and an alternative graphical approach. In our method, the y- and x-intercept of the plotted line provide the $K_1$ and $\lambda$, respectively, and the slope is the $-k_2$ applied to the two-compartment model.

### Validity of Two-Compartment Model

The scatter plot using Equation 3 should yield a straight line when the tracer kinetics are described by the two-compartment model. We observed a straight line in the human studies (Fig. 3), and a significant negative correlation between X(t) and Y(t) was obtained as r = −0.924 ± 0.062 and −0.882 ± 0.108 for normal subjects and patients, respectively. However, the delayed scan

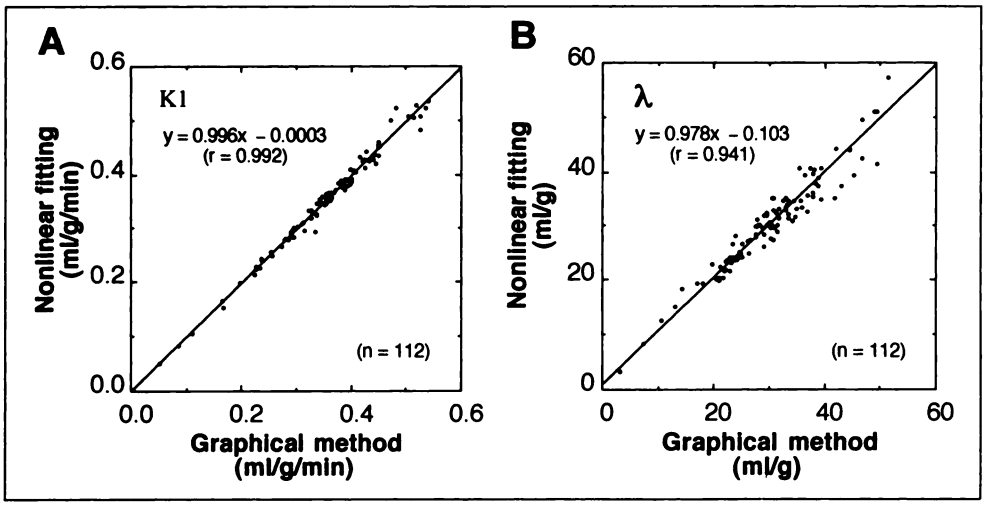


**FIGURE 6.** Comparison of $K_1$ and $\lambda$ obtained with the graphical method and the conventional nonlinear least-squares fitting technique in all subjects.

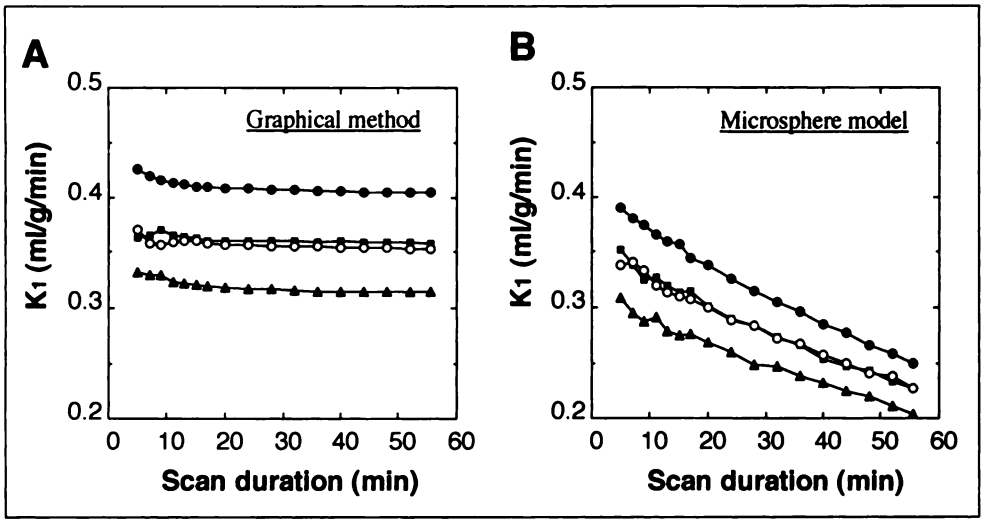


**FIGURE 7.** Time dependency of $K_1$ with IMP using the graphical method (A) and microsphere model (B) as means of all subjects (n = 14). ROIs were defined in the cerebellum (●), temporal cortex (○), parietal cortex (■) and frontal cortex (▲) in each of the two hemispheres. The estimated $K_1$ using the microsphere model was about 13% lower than that using the graphical method at 10 min.

data acquired at 210 min were slightly larger compared with the regression line from the data up to 57 min (Fig. 3). One possible explanation for the discrepancy is the nonlinearity caused by tissue heterogeneity (Fig. 9). We observed nonlinearity between X(t) and Y(t) using a computer simulation after a scan duration of 60–70 min. The discrepancy may also be due to the fact that the kinetics of IMP are described by the three-compartment model. Itoh et al. (*24*) estimated the value of $k_3$ to be 0.0057 ± 0.0131 $min^{-1}$ from the data up to 90 min. Nevertheless, they reported that the estimated $K_1$ by the three-compartment model was consistent with that by the two-compartment model: it makes little difference on $K_1$ within 60 min whether $k_3$ exists or not.

The values of $K_1$ using the graphical method should be independent of scan duration, assuming the two-compartment model is valid. The graphical method provided a constant $K_1$ (Fig. 7A), while the estimated $K_1$ using the microsphere model decreased as a function of scan duration (Fig. 7B). This is in agreement with results from a study by Murase et al. (*6*). Thus, the influence of washout from the brain was corrected using the graphical method. The relationship between the graphical method based on the two-compartment model (Eq. 3) and microsphere model (Eq. 4) was:

$$K_{1\ \text{graphical method}} = K_{1\ \text{microsphere}} + k_2X(t)$$

$$= K_{1\ \text{microsphere}} + \text{Correction factor for the washout.}$$

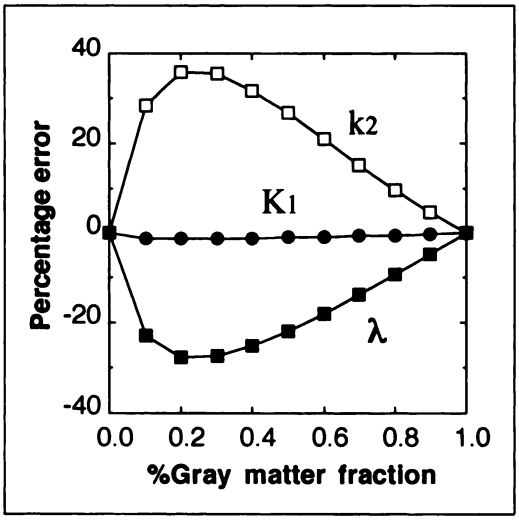


**FIGURE 8.** Percentage errors in estimated $K_1$, $k_2$ and λ due to tissue heterogeneity in the graphical method as a function of the gray matter fraction. The values of $K_1$ were assumed to be 80 ml and 20 ml/100 g/min in gray and white matter, respectively. The value for λ was 30 ml/g in both gray and white matter with a scan time of 60 min.

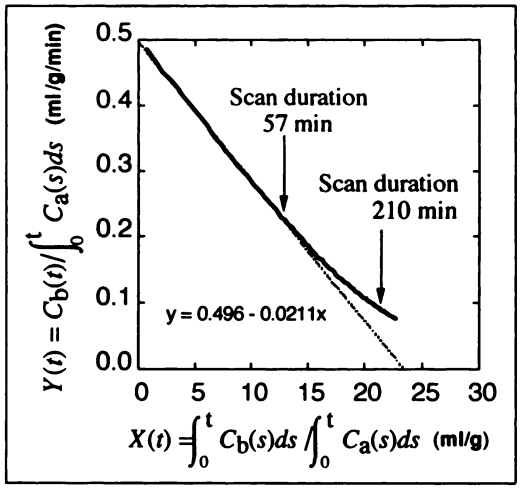


**FIGURE 9.** Effect of tissue heterogeneity on the graphical method with ranging scan times. The values of $K_1$ were assumed to be 80 ml and 20 ml/100 g/min in gray and white matter, respectively, and λ was 30 ml/g. The mixture of 50% gray and 50% white matter was assumed. The regression line (dotted line) was calculated using data from 0 to 60 min.

The $K_{1\ graphical\ method}$ is identical to the $K_{1\ microsphere}$ only if $k_2$ is assumed to be zero. In other words, if the microsphere model is valid, the regression line would be horizontal. Thus, the graphical method makes clear whether $k_2$ as well as $k_3$ exists and not only quantitates the value of $K_1$ but also evaluates the models validity.

We conclude that a two-compartment model was acceptable for IMP kinetics within a scan duration of 60 min.

### Validation of Estimated Flow Value

The values of $K_1$ using the graphical method should be compared with those using an independent method such as PET. In our comparative studies of IMP-SPECT and PET, the correlation between the $K_1$ with IMP and rCBF with $H_2{}^{15}O$ was good (r = 0.822) (Fig. 5). However, the $K_1$ with IMP was slightly lower compared to the rCBF with $H_2{}^{15}O$. Greenberg et al. (*5*) performed a comparison of IMP-SPECT with the $H_2{}^{15}O$ continuous infusion technique in seven normal subjects and showed that the rCBF obtained with IMP (47.3 ml/100 g/min) was slightly lower than that with $H_2{}^{15}O$ (57.6 ml/100 g/min). We previously obtained a rCBF of 48.4 ± 5.1 using dynamic PET and the $H_2{}^{15}O$ bolus infusion technique in the gray matter for four normal subjects (*25*). While performing the present IMP-SPECT studies with five normal subjects, we measured the average value of $K_1$ to be 41.3 ± 6.7 ml/100 g/min in the gray matter (Table 1). A reasonable explanation for underestimation with IMP is due to its limited extraction (*5*). The permeability surface area (PS) product of IMP was reported as 93.4 ml/100 g/min (*26*). Hence, the Renkin-Crone equation ($E = 1 - \exp(-PS/rCBF)$) (*27,28*) provided the extraction fraction E to be 0.85 at rCBF = 50 ml/100 g/min. Kuhl et al. (*2*) also reported that an increase in rCBF from 33 to 66 ml/100 g/min decreased the extraction fraction from 0.92 to 0.74.

We observed variations in $\lambda$ from the different brain regions (Fig. 6B). Kuhl et al. (*2*) suggested that the value of $\lambda$ varied with pH levels in the brain. Nishizawa et al. (*29*) demonstrated regional differences of uptake and retention of IMP, especially the slow increase and long retention of IMP observed in the basal ganglia. They suggested that regional characteristics were related to specific amine binding sites. Itoh et al. (*24*) observed a changed $\lambda$ in infarcted patients and suggested that the IMP binding mechanism may be related to tissue viability. However, the exact interpretation of $\lambda$ of IMP is not yet established.

### Accuracy of the Graphical Method

The values of $K_1$ and $\lambda$ estimated using the graphical method were in excellent agreement with those using the nonlinear least-squares fitting technique (r = 0.992 for $K_1$, r = 0.941 for $\lambda$; Fig. 6). The computer simulations showed the error on $K_1$ due to tissue heterogeneity to be negligible within 60 min (Fig. 9). The error in $K_1$ was less sensitive than that of $\lambda$ and $k_2$ (Fig. 8), and the same tendency was observed in our previous dynamic studies (*25,30*). Our results showed that the graphical method provided an accurate estimation of rCBF comparable to the conventional nonlinear least-squares fitting technique.

### Practical Advantage

The practical advantage of the graphical method is its rapid and simple computation compared to the conventional nonlinear least-squares fitting technique. The graphical method was about 20 times faster than the fitting technique for estimating $K_1$ and $\lambda$ because the iteration process is not included in this method. The graphical method is based on linear regression analysis and uses commercial spreadsheet software. Both $K_1$ and $\lambda$ can be calculated without knowledge of the nonlinear least-squares fitting technique. Thus, the graphical method is a simple way to solve nonlinearity problems in the two-compartment model. In this study, a relatively long scan time (57 min) was employed, but a scan time of 15–20 min was enough to estimate $K_1$ (Fig. 7A). Finally, the graphical method can be applied to another tracer described by the two-compartment (single tissue compartment) model.

## CONCLUSION

We have developed a graphical method to estimate rCBF and brain-blood partition coefficients based on a two-compartment model. This method was then applied to IMP-SPECT studies. We conclude that [$^{123}$I]IMP kinetics can be described by the two-compartment model within a scan time of 60 min and that the graphical method is a reliable strategy for estimating rCBF with [$^{123}$I]IMP and dynamic SPECT in clinical use.


## ACKNOWLEDGMENTS

We would like to thank the technical staff of the Department of Radiology and Nuclear Medicine, Research Institute for Brain and Blood Vessels Akita and Peter M. Bloomfield of the MRC Cyclotron Unit, Hammersmith Hospital for helpful discussion and advice in preparing this manuscript. This work was presented in part at the 39th Annual Meeting of the Society of Nuclear Medicine, Los Angeles, CA, 1992.


## REFERENCES


1. Winchell HS, Horst WD, Braun L, Oldendorf WH, Hattner R, Parker H. N-isopropyl [$^{123}$I]p-iodoamphetamine: single-pass brain uptake and washout; binding to brain synaptosomes; and localization in dog and monkey brain. *J Nucl Med* 1982;21:947–952.
2. Kuhl DE, Barrio JR, Huang SC, et al. Quantifying local cerebral blood flow by N-isopropyl-p(I-123) iodoamphetamine tomography. *J Nucl Med* 1982;23:196–203.
3. Matsuda H, Seki H, Sumiya H, et al. Quantitative cerebral blood flow measurements using N-isopropyl-(iodine 123)p-iodoamphetamine and single photon emission computed tomography with rotating gamma camera. *Am J Physiol Imaging* 1986;1:186–194.
4. Podreka I, Baumgartner C, Suess E, et al. Quantification of regional cerebral blood flow with IMP-SPECT: reproducibility and clinical relevance of flow value. *Stroke* 1989;20:183–191.
5. Greenberg JH, Kushner M, Rango M, Alavi A, Reivich M. Validation studies of iodine-123-iodoamphetamine as a cerebral blood flow tracer using emission tomography. *J Nucl Med* 1990;31:1364–1369.

6. Murase K, Tanada S, Mogami, et al. Validity of microsphere model in cerebral blood flow measurement using N-isopropyl-p-(I-123) iodoamphetamine. *Med Phys* 1990;17:79–83.
7. Kety SS. The theory and application of the exchange of inert gas at the lung and tissue. *Pharmacol Rev* 1951;3:1–41.
8. Kanno I, Uemura K, Miura S, Miura Y. HEADTOME: a hybrid emission tomography for single photon and positron emission imaging of the brain. *J Comput Assist Tomogr* 1981;5:216–226.
9. Hirose Y, Ikeda Y, Higashi Y, et al. A hybrid emission CT-HEADTOME II. *IEEE Trans Nucl Sci* 1982;NS-29:520–523.
10. Kanno I, Iida H, Miura S, et al. Design concepts and preliminary performance of stationary-sampling whole-body high-resolution positron emission tomography: HEADTOME IV. *Jpn J Nucl Med* [*Kakuigaku*] 1989; 26:477–485.
11. Iida H, Miura S, Kanno I, et al. Design and evaluation of headtome-IV, a whole-body positron emission tomograph. *IEEE Trans Nucl Sci* 1989; 36:1006–1110.
12. Yamamoto S, Amano M, Miura S, Iida H, Kanno I. Deadtime correction method using random coincidence for PET. *J Nucl Med* 1986;27:1925–1928.
13. Amano M, Iida H, Kanno I, Miura S, Hirose Y, Yamamoto S. A large-scale realtime-operation cache memory system installed in high resolution PET: preliminary results of realtime corrections of deadtime and decay and application to weighted integral method. *J Nucl Med* 1988;29(Suppl): 878.
14. Iida H, Kanno I, Inugami A, et al. Continuous-monitoring detector system of arterial $H_2{}^{15}O$ concentration for positron emission tomography: construction of the system and correction for the dispersion and the time-shift. *Jpn J Nucl Med* [*Kakuigaku*] 1987;24:1587–1594.
15. Iida H, Kanno I, Miura S, Murakami M, Takahashi K, Uemura K. Error analysis of a quantitative cerebral blood flow measurement using $H_2{}^{15}O$ autoradiography and positron emission tomography: with respect to the dispersion of the input function. *J Cereb Blood Flow Metab* 1986;6:536–545.
16. Kanno I, Iida H, Miura S, et al. A system for cerebral blood flow measurement using an $H_2{}^{15}O$ autoradiographic method and positron emission tomography. *J Cereb Blood Flow Metab* 1987;7:143–153.
17. Herscovitch P, Markham J, Raichle ME. Brain blood flow measured with intravenous $H_2{}^{15}O$. I. Theory and error analysis. *J Nucl Med* 1983;24: 782–789.
18. Raichle ME, Martin WR, Herscovitch P, Markham J. Brain blood flow measured with intravenous $H_2{}^{15}O$. II. Implementation and validation. *J Nucl Med* 1983;24:790–798.
19. Kanno I, Lammertsma AA, Heather JD, et al. Measurement of cerebral blood flow using bolus inhalation of $C^{15}O_2$ and positron emission tomography: description of the method and its comparison with the $C^{15}O_2$ continuous inhalation method. *J Cereb Blood Flow Metab* 1984;4:224–234.
20. Huang SC, Mahoney DK, Phelps ME. Quantitation in positron emission tomography: 8. Effects of nonlinear parameter estimation on functional images. *J Comput Assist Tomogr* 1987;11:314–325.
21. Gjedde A. High- and low-affinity transport of D-glucose from blood to brain. *J Neurochem* 1981;36:1463–1471.
22. Patlak CS, Blasberg RG, Fenstermacher JD. Graphical evaluation of blood-to-brain transfer constants from multiple-time uptake data. *J Cereb Blood Flow Metab* 1983;3:1–7.
23. Logan J, Fowler JS, Volkow ND, et al. Graphical analysis of reversible radioligand binding from time-activity measurements applied to [N-$^{11}$C-methyl]-(−)-cocaine PET studies in human subjects. *J Cereb Blood Flow Metab* 1990;10:740–747.
24. Itoh H, Iida H, Bloomfield PM, et al. A technique for a rapid imaging of regional CBF and partition coefficient using dynamic SPECT and I-123-amphetamine (IMP). *J Nucl Med* 1992;33(Suppl):911.
25. Yokoi T, Kanno I, Iida H, Miura S, Uemura K. A new approach of weighted integration technique based on accumulated images using dynamic PET and $H_2{}^{15}O$. *J Cereb Blood Flow Metab* 1991;11:492–501.
26. Murase K, Tanada S, Inoue T, et al. Measurement of the blood-brain barrier permeability of $^{123}$I IMP, $^{99m}$Tc HMPAO and $^{99m}$Tc ECD in the human brain using compartment model analysis and dynamic SPECT. *J Nucl Med* 1991;32(Suppl):911.
27. Renkin EM. Transport of potassium-42 from blood to tissue in isolated mammalian skeletal muscles. *Am J Physiol* 1959;197:1205–1210.
28. Crone C. The permeability of capillaries in various organs as determined by use of the indicator diffusion method. *Acta Physiol Scand* 1963;58: 292–305.
29. Nishizawa S, Tanada S, Yonekura Y, Fujita T, Mukai T, Saji H. Regional dynamics of N-isopropyl-($^{123}$I)p-iodo-amphetamine in human brain. *J Nucl Med* 1989;30:150–156.
30. Iida H, Kanno I, Murakami M, Takahashi K, Uemura K. A determination of the regional brain/blood partition coefficient of water using dynamic positron emission tomography. *J Cereb Blood Flow Metab* 1989;9:874–885.